



University of Parma Research Repository

There is plenty of asbestos at the bottom. The case of magnesite raw material contaminated with asbestos fibres

This is the peer reviewed version of the following article:

Original

There is plenty of asbestos at the bottom. The case of magnesite raw material contaminated with asbestos fibres / Gualtieri, Alessandro F; Malferrari, Daniele; Di Giuseppe, Dario; Scognamiglio, Valentina; Sala, Orietta; Gualtieri, Magdalena Lassinantti; Bersani, Danilo; Fornasini, Laura; Mugnaioli, Enrico. - In: SCIENCE OF THE TOTAL ENVIRONMENT. - ISSN 0048-9697. - 898:(2023), p. 166275. [10.1016/j.scitotenv.2023.166275]

Availability:

This version is available at: 11381/2967015 since: 2024-11-09T15:31:58Z

Publisher:

ELSEVIER

Published

DOI:10.1016/j.scitotenv.2023.166275

Terms of use:

Anyone can freely access the full text of works made available as "Open Access". Works made available

Publisher copyright

note finali coverpage

(Article begins on next page)

[Click here to view linked References](#)

1 **There is plenty of asbestos at the bottom. The case of magnesite raw**
2 **material contaminated with asbestos fibres**

3

4 Alessandro F. Gualtieri ^{ab}, Daniele Malferrari ^{ab*}, Dario Di Giuseppe ^a, Valentina Scognamiglio ^a,
5 Orietta Sala ^a, Magdalena Lassinantti Gualtieri ^c, Danilo Bersani ^d, Laura Fornasini ^d, Enrico
6 Mugnaioli ^e

7

8 ^a*Department of Chemical and Geological Sciences, University of Modena and Reggio Emilia, Via G. Campi 103,*
9 *41125 Modena, Italy*

10 ^b Inter-Departmental Research and Innovation Centre on Construction and Environmental Services of the
11 University of Modena and Reggio Emilia.

12 ^c*Department of Engineering "Enzo Ferrari", University of Modena and Reggio Emilia, Via Vivarelli 10, 41125*
13 *Modena, Italy*

14 ^d*Department of Mathematical, Physical and Computer Sciences, University of Parma, Parco Area delle Scienze 7/A*
15 *43124 Parma, Italy*

16 ^e*Department of Earth Sciences, University of Pisa, Via Santa Maria 53 56126 Pisa, Italy*

17

18 *Corresponding author, e-mail: daniele.malferrari@unimore.it

19

20 Science of the Total Environment

21 Submitted as **Research paper**

22

23 **ABSTRACT**

24 Although all six asbestos minerals (the layer silicate chrysotile and five chain silicate species
25 actinolite asbestos, amosite, anthophyllite asbestos, crocidolite and tremolite asbestos) are
26 classified as carcinogenic, chrysotile is still mined and used in many countries worldwide.
27 Other countries, like Italy, impose zero tolerance for all asbestos species but conflicting views
28 repress the development of globally uniform treaties controlling international trade of
29 asbestos-containing materials. Hence, countries with more severe legislations against the use
30 of these hazardous materials lack of an international safety net against importation of non-
31 compliant products. Raw materials that contain impurities of asbestos are challenging to
32 regulate and are examples of short-circuits of the global trading system, resulting in
33 embarrassing or disastrous situations. For the first time, we report the discovery of
34 commercial magnesite raw materials contaminated with white asbestos (chrysotile).
35 Magnesite is since decades used in countries like Italy for various industrial applications
36 without being aware of the asbestos impurity. The fibres observed in all samples analysed
37 have similar geometric parameters. The average length and width of the fibres are 6.0 and
38 0.11 μm , respectively, and the length value ranges from 0.62 to 56.7 μm , the width value from
39 0.01 to 0.06 μm . Quantitative analysis showed a chrysotile content around 0.01 wt.% not
40 allowed by current regulations in Italy and many other state. More generally, our findings
41 demonstrate that without shared policies aimed at regulating asbestos circulation on the
42 global market, “asbestos-free” national policies will inevitably fail. We call for the revision of
43 global directives on asbestos and implementation of standard analytical protocols for the
44 assessment of asbestos in natural raw materials to never again have another magnesite case.

45

46 *Keywords:* Magnesite, Asbestos, Chrysotile, REACH, Rotterdam Convention, Electron
47 microscopy.

48 **1. Introduction**

49 The term “asbestos” refers to the layer-silicate serpentine chrysotile (white asbestos) and
50 five double-chain silicates (amphiboles): actinolite asbestos, amosite (cummingtonite-
51 grunerite asbestos or brown asbestos), anthophyllite asbestos, crocidolite (riebeckite
52 asbestos or blue asbestos) and tremolite asbestos (Case et al., 2011). The International
53 Agency for Research on Cancer (IARC) classifies all the six asbestos species as “carcinogens
54 for humans” (IARC, 2012). Nevertheless, in contrast to the firm position taken by the IARC,
55 only the five amphibole asbestos species are globally banned, and many countries in the
56 world still allow the use of chrysotile (Gualtieri, 2017).

57 International treaties and agreements aimed at regulating the trade of hazardous
58 chemicals, including asbestos, have been stipulated. Due to disagreements over the use of
59 chrysotile and asbestos fibres concentration limits a globally harmonized system is still
60 lacking. Chrysotile remains a mineral of high socio-economic and industrial relevance as in
61 many countries it still represents an important economic resource and its hazardousness is
62 unrecognised or, at the very least, ignored. In addition, even in states where chrysotile has
63 been banned, it is not easy to verify the coupling between government ratification of
64 international conventions and successful enforcement of the ban (Joshi et al., 2006; Lin et al.,
65 2019; Yoon et al., 2018), although feedbacks in many cases are from monitoring activities
66 such as, for example, the implementation of policies for the search for asbestos substitutes,
67 the enforcement of the national surveillance system of the incidence of mesothelioma, and the
68 control over the removal of and its eventual transformation into End-of-Waste (Aryal and
69 Morley, 2020; Chimed-Ochir et al., 2022; Marsili et al., 2017; Thives et al., 2022). In the face of
70 these challenges, it is not surprising that the governing body of the Rotterdam Convention for
71 Hazardous Chemicals has not yet managed to reach consensus for listing chrysotile in Annex
72 III and thus compel producers to label chrysotile. This excellent tool for international trade

73 control of dangerous chemicals is thus not available for chrysotile. It should be remarked that
74 the inclusion of a chemical in the Rotterdam convention requires a unanimous vote of all the
75 countries is needed, and only a handful of supplier or user countries block this.

76 In the European Union, the REACH compliance prohibits any intentional use of asbestos,
77 but allows the presence of category 1A carcinogens, including asbestos fibres, as contaminant
78 in concentrations <0.1wt.% without obligation of labelling. Both the Rotterdam Convention
79 and the REACH compliance are in contrast with more severe domestic laws of some parties
80 like Italy that applies “zero tolerance” (Dlg 257/92, 1992) for asbestos fibres; this means that
81 the unauthorised supply, transport, use, including manufacture and handling of asbestos and
82 any material containing asbestos, even in trace, is prohibited. Direct consequences of these
83 legislative disagreements are that asbestos-containing materials (ACMs) may be unknowingly
84 imported and used in countries that have banned all asbestos minerals. An even more
85 complicated situation occurs when asbestos fibres are present as contaminants, perhaps even
86 accidentally. This situation can occur in the exploitation of certain minerals that may contain
87 impurities of naturally occurring asbestos (Gualtieri, 2020).

88 In this scenario, our research group has been working for several years in screening
89 natural raw materials that potentially contains asbestos. Our work is strictly voluntary and
90 motivated by the scientific conviction that only zero exposure of workers and the population
91 is a guarantee for the elimination of asbestos-related health issues. The methodology of this
92 environmental surveillance includes follow-up on reports and notifications from mining
93 companies as well continuous survey of existing literature to uncover cases of raw materials
94 contaminated with asbestos. Knowing the specific rock types and geologic conditions leading
95 to the formation of asbestos, potentially contaminated mineral commodities can be identified.
96 These include Mg-rich silicates like serpentized olivine (Van Gossen et al., 2003),
97 vermiculite (Addison, 1995; Larson et al., 2010) and many more although, over the years,

98 special concerns have been raised about potential human exposure and risk from asbestos in
99 consumer products containing cosmetic talcum powder, especially its use with infants (Burns
100 et al., 2019; Emory et al., 2020; Finley et al., 2012; Fitzgerald et al., 2019; Gordon et al., 2014;
101 Van Gossen et al., 2003).

102 Hitherto, our activity contributed to disclose the case of a Na-feldspar mined in Orani
103 (Sardinia, Italy) contaminated with asbestos tremolite (Gualtieri et al., 2018) and the case of
104 commercial chrysotile-rich brucite from China, where the use of chrysotile asbestos is allowed
105 (Malferrari et al., 2021). In the case of the Orani feldspar, mined since 1970, the presence of
106 asbestos was discovered in 2015 and the mining activity, in compliance with Italian law, was
107 consequently stopped. Our work contributed to assess unequivocally the nature of the
108 asbestos fibres as tremolite and to recommend a safe selective exploitation of the 'asbestos
109 free' raw material (Gualtieri et al., 2018). In the case of the Chinese brucite (Malferrari et al.,
110 2021), the Italian import flow was promptly halted and the processing sites were cleared,
111 thus avoiding future legal and, most importantly, health complications.

112 Recently we discovered that magnesite (MgCO_3), a widespread industrial raw material,
113 may be contaminated with asbestos. Magnesite is used in several industrial applications such
114 as the production of insulating materials and coatings, as inorganic additive in ceramic inks,
115 pigments and cements, for CO_2 sequestration and as MgO source. This mineral can be
116 associated with serpentine (Tzamos et al., 2020) and eventually also with asbestos minerals
117 when occurring in altered ophiolitic rocks (i.e., outcrops of basic/ultrabasic rocks
118 representing relicts of oceanic crust or upper mantle). In fact, magnesite occurs in four types
119 (Drnek et al., 2018; Pohl, 1990): (i) of sedimentary origin within ancient marine platform
120 carbonate suites (Veitsch type); (ii) in ultramafic magmatic rocks (Kraubath type); (iii) in
121 sedimentary fluvial-limnic sediments overlying ultramafics (Bela Stena type); (iv) in
122 metamorphosed ultramafics with high magnesite content (Greiner type). Sedimentary type (i)

123 is assumed not to contain asbestos minerals while type (iii) and (iv) are of minor economic
124 importance. On the contrary, the Kraubath type deposits are actively exploited and may
125 contain asbestos minerals formed as a result of lithological transformation processes (see
126 [Supporting information](#) for further details).

127 In this work, we report the results of a systematic investigation of samples of magnesite
128 from Kraubath type deposits imported from Turkey (KT) and Greece (KG) for use in the
129 Italian production of traditional ceramics. In the title of the paper, we have chosen to
130 paraphrase the famous title of the lecture given by Richard Feynman at the annual American
131 Physical Society meeting in 1959 to point out that asbestos is still among us and circulates in
132 an insidious way. It is essential to bear in mind that magnesite, if uncontaminated, poses no
133 risk. When, on the other hand, it is contaminated with asbestos even at low concentrations, in
134 addition to being illegal in many states, it poses a serious health risk, as shown by the
135 numerous studies on chrysotile toxicity (see Gualtieri, 2023 for a recent review).

136

137 **2. Materials and Methods**

138

139 *2.1. Samples*

140 Representative samples of magnesite from Kraubath type deposits imported from Turkey
141 (KT) and Greece (KG) and used in Italian manufacture sites of traditional ceramics have been
142 investigated. The geological description of the two areas is reported in the [Supporting](#)
143 [Information](#). Both fine powders (KT1 and KG1) and lumps (KT2 and KG2) from the same
144 deposits have been analysed. The samples were collected from distributors as well as from
145 industrial end-users. A granulated commercial product of sedimentary Veitsch type from
146 Austria, from now on called VA, was also included in the investigation together with various
147 brands of commercial fine magnesite powders sold by Italian sporting goods retailers as anti-

148 slip agent for various sports activities such as climbing. Among these powders, a commercial
149 hydro-magnesite was also included.

150

151 *2.2 X-ray powder diffraction*

152 The mineralogical characterization of the magnesite samples was performed by X-Ray
153 Powder Diffraction (XRPD) using an X'Pert-PRO PANanalytical θ/θ diffractometer (CuK α
154 radiation, 40kV and 40 mA), equipped with a Real Time Multiple Strip detector and Ni filter on
155 the secondary beam. Data were collected from 3 to 80 °2 θ , with a virtual scan time of 5s/step
156 and step scan of 0.0167 °2 θ . The XRPD spectra were preliminary analysed using the X-Pert
157 High Score Plus software. A 1/2° divergence slit and a 0.2 mm receiving slit were used. The
158 quantitative mineralogical analysis was performed with the Rietveld method (Rietveld, 1969)
159 using the General Structure Analysis System (GSAS) software package (Larson and Von
160 Dreele, 1994) with the graphical interface EXPGUI (Toby, 2001) and following the protocol
161 reported in Gualtieri et al. (2019). More in detail, XRPD patterns background was modelled
162 using a Chebyshev polynomial of the first kind, peak shapes were modelled using the
163 Thompson–Cox–Hastings pseudo-Voigt function, and March-Dollase function was chosen as
164 intensity correction factor for preferred orientations and applied to the reflections (104) of
165 magnetite and (001) of serpentine. The starting structural models used for the refinement are
166 from Graf (1961) for magnesite, Gualtieri (2000) for quartz, Steinfink and Sans (1959) for
167 dolomite, Ondrus et al. (2003) for calcite, Lister and Bailey (1967) for chlorite and Manceau et
168 al. (1998) for smectite. Lizardite from Mellini (1982) was chosen as the starting structural
169 model for quantitative estimation of serpentine.

170

171 *2.3 Thermal analyses and evolved gasses mass spectrometry*

172 Thermogravimetric (TGA) and thermo-differential (DTA) analyses were performed with a
173 Seiko SSC 5200 thermal analyser coupled with quadrupole mass spectrometer (ESS, GeneSys
174 Quadstar 422) to detect gases released during thermal reactions (MSEGA). Gas sampling was
175 done using a silicon capillary pre-heated to avoid gas condensation. Experimental conditions
176 were: heating rate: 20 °C/min; heating range: 25-1000 °C; TGA and DTA data measurement:
177 every 0.5 s; DTA reference: α -alumina powder; purging gas: ultrapure helium with a flow rate
178 of 100 μ L/min. Mass analyses were performed in multiple ion detection mode by measuring
179 m/z ratios (i.e., the dimensionless ratio of the mass number m to the z-charge of an ion) 18,
180 30, 44, 64 to detect the emission of H₂O, NO, CO₂, and SO₂, respectively using a secondary
181 electron multiplier (SEM) detector set at 900 V with 1 s integration time on each measured
182 mass.

183

184 *2.4 Optical microscopy analyses*

185 Preliminary observation of the raw sample (KT2) with A Meiji Techno stereomicroscope
186 (50x) showed that the green veins are characterised by an intergrowth of green plate-like
187 mineral grains with bundles of white mineral fibres with a length between 0.5-0.7 mm. Fibres
188 were picked up using tweezers and subsequently characterised with Phase Contrast Optical
189 Microscope (PCOM). PCOM analyses were conducted following the methodology proposed by
190 Di Giuseppe et al. (2021) for the identification of chrysotile. Analyses were carried out using
191 an Olympus BX51 phase-contrast microscope and Cargille Refractive Index (RI) Liquid n =
192 1.550. Two drops of refractive index medium were placed on a pre-cleaned glass slide (76×26
193 mm). Few representative fibres or bundles were placed on the slide and covered with a cover
194 slip. PCOM observations were made in both phase contrast and dark field mode. The PCOM
195 technique was not applied to powder magnesite samples due to the small size of the fibres in
196 these samples.

197

198 *2.5 Electron microscopy*

199 The morphological observation of the samples was carried out by a Scanning Electron
200 Microscope (SEM) using JSM-6010PLUS/LA (JEOL, Hillsboro, OR, USA) equipped with an
201 Energy Dispersive X-ray (EDX) microanalysis system (Oxford INCA-350) and Field Emission
202 Gun Scanning Electron Microscope (FEG-SEM) FEI Nova NanoSEM 450 FEG-SEM. According
203 with the Italian Minister Decree 06.09.94 (DM September 06, 1994) the procedure for
204 quantitative SEM analysis was performed as follows: an amount of 5 mg of the sample was
205 suspended in 200 ml of deionized water with 0.1 vol.% surfactant additive (dioctylsodium
206 sulfocinate, $C_{20}H_{37}NaO_7S$, CAS no. 577-11-7), and ultrasonicated for 10 min to promote
207 particle separation. A volume of 6 ml of this suspension was collected at different levels in a
208 becker and placed in a filtration system, allowing random deposition of the particles on
209 polycarbonate filters (20 mm² surface, 0.45 μ m porosity). Then the filter was dried at 55 °C
210 and weighed. The final weight of the material deposited on the filter was 0.1 mg. The filter
211 was mounted on an aluminium stub and coated with gold using a Carbon Coater-Balzers CED-
212 010 (10 nm thick). The SEM images were obtained by secondary electron imaging covering 1
213 mm² of surface at 4000 \times magnification (130 analysis fields).

214 The powder samples KT1 and KG1 were investigated as received while small fragments of
215 the raw KT2 and KG2 samples were gently ground in agate mortar to obtain a fine powder. A
216 small amount of sample was suspended with 1 mL of ethanol in a test tube, sonicated for 1
217 min (using a low power sonic bath) and left to set for 5 min. A drop of the suspension was
218 then transferred and dried onto a 300-mesh carbon copper TEM grid.

219 Preliminary TEM investigations focused on the microstructure of the mineral fibres in the
220 samples were carried out at the CIGS-UNIMORE laboratories by using a Talos F200S G2

221 microscope, equipped with S-FEG Schottky field emitter operating at 200 kV and two large-
222 area EDX spectrometers with Silicon Drift Detectors (SDD).

223 High resolution transmission electron microscopy (HRTEM), energy-dispersive X-ray
224 spectroscopy (EDS) and three-dimensional electron diffraction (3DED) were performed with
225 a JEOL JEM-F2000 Multi-purpose, working at 200 kV and equipped with Schottky-FEG source
226 and SDD EDS detector. 3DED data were analysed and visualized by ADT3D software (Gemmi
227 et al., 2019; Kolb et al., 2011).

228

229 *2.6 Micro-Raman spectroscopy*

230 The Raman spectra were collected on the magnesite powders (KT1 and KG1) and on a
231 fragment (KT2) with a HORIBA Jobin Yvon LabRam confocal micro-spectrometer (300 mm
232 focal length), using a He-Ne 632.8 nm and a frequency doubled Nd:YAG 473.1 nm laser lines
233 as excitation sources, with an integrated Olympus BX40 microscope with 4×, 10×, 50× ULWD
234 and 100× objectives, a 1800 grooves/mm grating, a XY motorized stage and a Peltier cooled
235 silicon CCD. The spectral resolution is $\sim 2\text{ cm}^{-1}$ with the 632.8 nm line and $\sim 4\text{ cm}^{-1}$ with the
236 473.1 nm line. The system was calibrated by using the 520.6 cm^{-1} Raman peak of silicon in the
237 low-wavenumber spectral region ($100\text{-}1200\text{ cm}^{-1}$) and the emission lines of a gas lamp in the
238 high-wavenumber spectral region ($3000\text{-}4000\text{ cm}^{-1}$). The spectra have been recorded with
239 typical exposures of 60 s repeated at least 4 times. Data analysis has been performed by
240 LabSpec 5 built-in software. Fit with bands deconvolution has been carried out with Gauss-
241 Lorentzian functions.

242

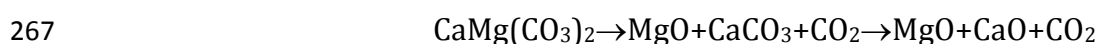
243 **3. Results**

244 The XRPD data on the magnesite samples show a number of secondary phases ([Table 1](#)).
245 The mineralogical composition (wt%) of samples KT1 and KG1, performed using Rietveld's

246 quantitative phase analysis (Fig. 1 and Table 2), revealed magnesite, quartz, serpentine and
247 dolomite in sample KT1, while talc, calcite, smectite and chlorite were also identified in
248 sample KG1.

249 In addition to the magnesite decarbonation, the TGA/DTA-MSEGA analyses highlight, in
250 samples polluted with chrysotile, the typical dehydroxylation reaction of the octahedral sheet
251 of chrysotile followed by an exothermic event indicating its recrystallization in forsterite
252 (Bloise et al., 2016; Cattaneo et al., 2003; Khorami et al., 1984). For both KT1 and KG1, the
253 TGA curves and their first derivative (DTG) show one principal (1) and one minor (2) thermal
254 event, which are both attributed to multiple fully or partially overlapping thermal reactions.
255 An additional thermal event (3) is evidenced by the DTA curve, but only for KT1.

256 In KT1 (Fig. 2a) reaction (1) occurs in the temperature range 445-640 °C (maximum
257 reaction rate at 599 °C) and results in a mass loss of 42.1 wt%. Reaction (2), which occurs
258 between 650 and 735 °C is less evident and produced a mass loss of 1.0 wt%. The DTA curve
259 (Fig. 2b), in addition to the endothermic signals related to reactions (1) and (2), also
260 highlights a weak exothermic reaction (3) with a maximum at about 830 °C. The release of CO₂
261 (m/z=44, Fig. 2c) associated with reaction (1) proves that this thermal event occurs following
262 the decarbonation of magnesite (mainly) and of dolomite (first step). On the other hand,
263 reaction (2) involves the simultaneous release of H₂O (m/z=18, Fig. 2c) and CO₂ that could be
264 respectively related to the dehydroxylation of the serpentine and to the second step of
265 dolomite decarbonation according to the well-known thermal decomposition mechanism
266 (Bloise et al., 2016):



268 where the first step is not distinguishable as completely overlapping with reaction (1).

269 Reaction (3) is due to the recrystallization of the serpentine in forsterite occurring after
270 dehydroxylation (Bloise et al., 2016; Cattaneo et al., 2003; Khorami et al., 1984). Below 250 °C,

271 it is also possible to observe weak reactions, more evident in the magnification of [Fig. 2a](#) and
272 in MSEGA curve $m/z=18$ ([Fig. 2c](#)), related to the removal of more or less strongly bound water
273 molecules.

274 The thermal behavior of sample KG1 nearly parallels that of KT1 and is described in the
275 [Supporting Information](#).

276 Macroscopic fibre bundles were discovered in the raw rock samples. For example, the
277 macroscopic observation of the raw KT2 sample composed of centimetric rock fragments ([Fig.](#)
278 [3a](#)) shows green lamellar mineral phases and white mineral fibres ($L= 0.5\text{--}0.7$ mm). The latter
279 were selected and observed with PCOM and revealed beautiful bundles of chrysotile fibres
280 ([Fig. 3b](#)). The PCOM technique allowed to easily identify the nature of the fibres in KT2. In
281 fact, fibres treated with $RI=1.550$ liquid displayed the characteristic dispersion colours of
282 chrysotile (Di Giuseppe et al., 2021). Observed in phase contrast mode, fibres colour was light
283 blue with an orange halo when the fibre axis was perpendicular to the polariser, and dark blue
284 with an orange halo when the fibre axis was parallel to the polariser ([Fig. 3b](#)).

285 The SEM images of raw and powder magnesite samples from Turkey (KT1, KT2) and
286 Greece (KG1, KG2) show a matrix of massive magnesite particles with several flexible bundles
287 of chrysotile fibres ([Fig. 4a-d](#)) whose nature has been confirmed by the EDX analyses ([Fig. 4](#)
288 [e,f](#)). A series of representative SEM images were analysed using *ImageJ* software, which
289 provides accurate measurements of the length and width of the chrysotile fibre. The fibres
290 observed in the Turkish (KT1) and Greek (KG1) powders samples have the same geometrical
291 parameters. The average fibre length and width are 6.0 and 0.11 μm respectively. The length
292 value ranges from 0.62 to 56.7 μm , the width from 0.01 to 0.06 μm .

293 Most of the fibres display the so-called “Stanton size”: based on *in vivo* animal studies,
294 asbestos fibres longer than 8 μm and thinner than 0.25 μm are strongly carcinogenic and
295 induce malignant pleural mesothelioma (Stanton et al., 1981; Stanton and Wrench, 1972). The

296 quantitative SEM analysis carried out according to the Italian Ministry of Health regulations
297 and technical methodologies (DM September 06, 1994) highlighted a chrysotile content of
298 0.012 wt.% for KT1 (0.012 wt.% for KT2 and 0.010 wt.% for the KG samples).

299 TEM observations confirm that chrysotile is the fibrous phase present in the investigated
300 Turkish and Greek magnesite samples. In particular, sample KT2 contains fibres long up to
301 few microns and thick up to 80 nm (Fig. 5a). A closer look reveals that these fibres have a
302 nanotube structure, with internal channels that may be more or less visible and large up to
303 30-40 nm (Fig. 5b). More massive fragments are also present in the KT2 sample, although
304 with a significantly lower incidence. EDS measurements show that both fibres and massive
305 fragments have a comparable composition, consistent with serpentine minerals (Fig. 5c).
306 3DED analysis confirms that the fibres are chrysotile; the reconstructed diffraction volume
307 shows typical crowns of diffuse scattering produced by the bending of the serpentine layers
308 (Fig. 5d). 3DED also reveals that massive fragments consist of lizardite or polygonal
309 serpentine; the latter is easily recognizable due to the circular crowns of reflections arranged
310 according to a pseudo five-fold symmetry (Fig. 5e) (Baronnet et al., 1994). All the other
311 samples consist mostly of magnesite crystals of different size. Elongated tubular fibres are
312 also spotted very frequently. Some fibres display a habit similar to the chrysotile detected in
313 sample KT2, but the most common form consists of bent hair-like fibres typically arranged in
314 crowded bundles (see for example the chrysotile fibres in sample KG2 reported in Fig. 5f).

315 The Micro-Raman data confirm the results obtained with the other experimental
316 techniques. The signal of chrysotile was detected in both Turkish and Greek samples. In the
317 Turkish powder KT1, lizardite was also observed, and its signal sometimes appears in
318 conjunction with that of chrysotile. In the low-wavenumber spectral range, the Raman signals
319 related to the lattice vibrational modes and the internal vibration of the SiO₄ tetrahedra of a
320 serpentine phase were observed in KT1 (at 229, 385, 619, 690 cm⁻¹) and in KG1 (at 392, 689

321 cm^{-1}) (Fig. 6a). The contribution of magnesite from the surrounding crystals was also detected
322 (at 211, 329, 738, 1094 cm^{-1}) (Fig. 6a). The univocal identification of chrysotile in the powders
323 was confirmed by its peculiar Raman bands of the OH stretching vibrations (Fornasini et al.,
324 2022), between 3500-3800 cm^{-1} , with an intense peak at $\sim 3695 \text{ cm}^{-1}$ and a weak contribution
325 at $\sim 3647 \text{ cm}^{-1}$ (Fig. 6b). Typically, the most intense peak of chrysotile is also characterized by
326 a shoulder at $\sim 3680 \text{ cm}^{-1}$, which is markedly pronounced in KT1. A possible contribution due
327 to lizardite, in addition to chrysotile, may explain this curve shape, since its most intense OH
328 stretching signal occurs at 3683 cm^{-1} (Auzende et al., 2004; Petriglieri et al., 2015). The
329 presence of chrysotile in KT1 was supported by the analysis on the raw fragment (KT2),
330 whose Raman spectrum corresponds to that of chrysotile (characteristic peaks occurring at
331 233, 391, 691 and 1104 cm^{-1} in the low-wavenumber range and at 3697 with a shoulder at
332 $\sim 3687 \text{ cm}^{-1}$ in the OH stretching region).

333

334 **4. Discussion**

335 Our systematic investigation clearly shows that a small amount of chrysotile is present as
336 the only asbestos phase in the Kraubath type industrial minerals from Greece and Turkey. The
337 Austrian granulate of sedimentary Veitsch type (VA) as well the powders sold at retail as anti-
338 slip agent do not contain asbestos at all. We rule out the possibility of contamination during
339 materials processing of the industrial minerals as chrysotile fibres were found in both the
340 powders and the raw fragmented rocks. Only the use of a suite of different experimental
341 techniques made it possible to assess indisputably that chrysotile is present in these
342 magnesite products. In this context, XRPD and TGA/DTA are inconclusive methods while
343 micro-Raman and electron microscopy techniques are decisive for revealing the true crystal-
344 chemical nature of the fibres. Fine powders are particularly challenging and high-resolution
345 electron microscopy analyses of carefully prepared specimens are indispensable for revealing

346 the presence of fibre bundles. Hence, even actors in the supply chain that have actively
347 searched for asbestos contaminants may have failed due to inadequate analysis methods.
348 Together with the lack of adequate and shared analytical protocols, this could be a reason why
349 chrysotile was not revealed before by the magnesite producers.

350 In Italy, this magnesite product has been used as raw material in the traditional ceramics
351 industry for decades without being aware of the asbestos contaminant. Our discovery reveals
352 major flaws in the global network and a number of violations and conflicts. Regarding the
353 violations, asbestos contaminated magnesite should be considered as illicit in countries like
354 Italy, Germany and France where the marketing of all ACMs, with a few exceptions, where
355 banned during the 90s (Décret 96-1133, 1996; dlg 257/92, 1992; Gesetz 162, 1993). This
356 applies also to industrial minerals where asbestos has not been intentionally added even in
357 very low concentration. There is also a violation of the 2009 European directive (EC
358 2009/148, 2009) on the protection of workers from the risks related to exposure to asbestos
359 at work as *“Even though it has not yet been possible to identify the exposure threshold below
360 which asbestos does not involve a cancer risk, occupational exposure to workers to asbestos
361 should be reduced to a minimum.”* Another violation regards the fact that, according to the
362 2006 EU Regulation (EC 2006/1907, 2006), all articles containing asbestos must bear the
363 “asbestos” label. Unfortunately, a number of conflicts and discrepancies make the actual
364 situation chaotic. The 2006 EU Regulation specifically prohibits the placing on the market of
365 articles and mixtures containing asbestos fibres *“added intentionally”*. Because chrysotile is
366 not added intentionally to magnesite but is a natural contaminant, is this “article” out of the
367 2006 EU Regulation? The same Regulation admits a content of carcinogens, including
368 asbestos, of 0.1 wt%. In this case, the Turkish magnesite powder (KT1) for example, with a
369 chrysotile content of 0.012 wt.%, would be legal in the EU.

370 Regarding importation from extra-EU countries, the Rotterdam convention is a precious
371 tool for the adhering parties (including EU countries) in avoiding accidental importation of
372 domestically forbidden substances. In fact, the Rotterdam Convention deals with “*substances*
373 *whether by itself or in a mixture ...*” (Article 1) with no specification of the quantity except for a
374 generic statement on “*...chemicals in quantities not likely to affect human health...*” (Article 3);
375 the latter, however, is not the case though because it is well known that there is no evidence
376 for a threshold or a “safe” level of asbestos exposure (see for example, Lemen and Landrigan,
377 2017). Each party is obliged to guarantee that exporters within its jurisdiction do not ship
378 listed chemical to other parties that disapproves importation of them. This multilateral treaty
379 regulates the international trade of hazardous chemicals, listed in Annex III to the convention.
380 Whereas amphibole asbestos species are listed, chrysotile is still only recommended for
381 listing by the Chemical Review Committee. The outcome is that legal responsibilities shift
382 from exporters to importers, with an obvious increased risk of finding non-compliant
383 products on the European market. Hence, in countries like Italy, asbestos contaminated
384 magnesite is automatically out of law only when it is already present in its territory.

385 This chaos in the global market of ACMs has negative consequences for countries that
386 wish to protect people from any exposure to asbestos fibres. For example, workers handling
387 industrial raw materials containing unknown asbestos contaminants do not make adequate
388 use of protective measures and the exposure risk increases (Burdett and Bard, 2007; Douglas
389 and Van den Borre, 2019). The Individual companies can suffer from severe economic losses
390 and legal issues if the presence of ACMs is discovered by the local environmental/health
391 authorities. The site can be impounded by a state’s attorney with the suspension of the
392 working activity and access prohibited until the end of the legal action. This was the case with
393 the Italian feldspar mine contaminated with tremolite asbestos (Gualtieri et al., 2018).

394 It is sad to acknowledge that countries (like Italy) hardly targeting to turn “asbestos-
395 free” (Terracini, 2019) or at least “asbestos-safe” see their efforts thwarted by the income of
396 new contaminated materials on their territory without their knowledge.

397

398 **5. Conclusions**

399 The global use of asbestos is decreasing worldwide (Frank and Joshi, 2014) but is still
400 not zero. Naturally occurring asbestos (Gualtieri, 2020) is another threat to the public health
401 that transforms from local to geographically widespread when the fibres are present as
402 impurity in industrial minerals that may freely circulate among states seriously impacting the
403 total environment. The magnesite case reported here is a perfect example of this type of
404 situation and proves that there is still plenty of asbestos at the bottom. Our research group
405 will continue the screening of commercial raw materials in search of asbestos for predictive
406 purposes. We have to avoid *ex post* discovering of the exposure of the population or workers
407 to some mineral source through the observation of malignant mesothelioma morbidity peaks
408 as was the case in the past for fluoro-edenite in Biancavilla (Italy) (Comba et al., 2003) or
409 fibrous erionite in Cappadocia (Turkey) (Baris et al., 1987).

410 In concrete terms, we believe that without a global ban of asbestos (Douglas and Van
411 den Borre, 2019), which appears to be utopic at the moment, only shared harmonized policies
412 aimed at regulating asbestos mining and circulation adopted by all the countries that have
413 banned asbestos and that aspire to become asbestos-free can drive us to see the light at the
414 end of the tunnel. We call for a harmonized standard analytical protocol: when imported, each
415 raw material and especially those of asbestos-compatible origin, must be accompanied by a
416 certification of absence of asbestos phases, assessed by a suite of analytical determination
417 also including high-resolution SEM or TEM, that producers (the mining companies) deliver.
418 The importing company/national distributors can randomly cross-check the reliability of the

419 certificates by validated specialized labs using the analytical methodologies mentioned above.
420 Following the case of the talc mining industry (Schlossman, 2009) and the example of New
421 Caledonia where the exploitation of serpentine rocks contaminated by asbestos is strictly
422 regulated (Worliczek, 2017), mining activity in asbestos-rich or supposedly asbestos-rich
423 national deposits should be always carried out under severe monitoring and differential
424 processing to avoid exploitation of asbestos-rich levels. As for the case above, the domestic
425 distribution of the raw materials delivered to the production sites must be accompanied by a
426 certification of absence of asbestos phases.

427 The conflict between the European REACH compliance (EC 2006/1907, 2006) that
428 admits a content of carcinogens, including asbestos, of 0.1 wt% in circulating raw materials,
429 and the national laws must be resolved by making an exception for asbestos in the list of
430 REACH carcinogens so that, compatible with the SEM experimental detection limits, the raw
431 materials should not contain asbestos phases.

432 Finally, at a global level, we call for the inclusion of chrysotile in the list of Rotterdam
433 convention of Hazardous Chemicals under the Rotterdam Convention to be labelled for
434 import/export operations.

435

436 **CRedit authorship contribution statement**

437 Alessandro F. Gualtieri: Supervision, Project administration, Conceptualization, Resources,
438 Formal analysis, Methodology, Validation, Writing the original draft, Writing, review and
439 editing, Funding acquisition. Daniele Malferrari: Supervision, Methodology, Validation,
440 Writing, review and editing, Funding acquisition. Dario Di Giuseppe: Investigation, review and
441 editing. Valentina Scognamiglio: Investigation, review and editing. Orietta Sala: Investigation,
442 review and editing. Magdalena Lassinantti Gualtieri: Conceptualization, Writing the original
443 draft, Writing, review and editing. Danilo Bersani: Investigation, Writing – review and editing.

444 Laura Fornasini: Investigation, Writing – review and editing. Enrico Mugnaioli: Investigation,
445 Writing – review and editing.

446

447 **Acknowledgments**

448 The work is supported by the PRIN project fund “Fibres: a multidisciplinary mineralogical,
449 crystal-chemical and biological project to amend the paradigm of toxicity and cancerogenicity
450 of mineral fibres” (PRIN: Progetti di Ricerca di Rilevante Interesse Nazionale—Bando 2017—
451 Prot. 20173X8WA4). Authors thanks the Center for Instrument Sharing of the University of
452 Pisa (CISUP), Italy, for the TEM measurements.

453

454 **Data availability**

455 Data will be made available on request.

456

457 **Declaration of competing interest**

458 The authors declare that they have no known competing financial interests or personal
459 relationships that could have appeared to influence the work reported in this paper.

460

461 **References**

- 462 Addison, J., 1995. Vermiculite: a review of the mineralogy and health effects of vermiculite
463 exploitation. *Regul. Toxicol. Pharmacol.* RTP 21, 397–405.
464 <https://doi.org/10.1006/rtp.1995.1054>
- 465 Aryal, A., Morley, C., 2020. Call for a global ban policy on and scientific management of asbestos to
466 eliminate asbestos-related diseases. *J. Public Health Policy* 41, 279–285.
467 <https://doi.org/10.1057/s41271-020-00223-4>
- 468 Auzende, A.-L., Daniel, I., Reynard, B., Lemaire, C., Guyot, F., 2004. High-pressure behaviour of
469 serpentine minerals: a Raman spectroscopic study. *Phys. Chem. Miner.* 31, 269–277.
470 <https://doi.org/10.1007/s00269-004-0384-0>
- 471 Baris, I., Simonato, L., Artvinli, M., Pooley, F., Saracci, R., Skidmore, J., Wagner, C., 1987. Epidemiological
472 and environmental evidence of the health effects of exposure to erionite fibres: a four-year
473 study in the Cappadocian region of Turkey. *Int. J. Cancer* 39, 10–17.
474 <https://doi.org/10.1002/ijc.2910390104>
- 475 Baronnet, A., Mellini, M., Devouard, B., 1994. Sectors in polygonal serpentine. A model based on
476 dislocations. *Phys. Chem. Miner.* 21. <https://doi.org/10.1007/BF00202098>

477 Bloise, A., Catalano, M., Barrese, E., Gualtieri, A.F., Bursi Gandolfi, N., Capella, S., Belluso, E., 2016.
478 TG/DSC study of the thermal behaviour of hazardous mineral fibres. *J. Therm. Anal. Calorim.*
479 123, 2225–2239. <https://doi.org/10.1007/s10973-015-4939-8>

480 Burdett, G., Bard, D., 2007. Exposure of UK Industrial Plumbers to Asbestos, Part I: Monitoring of
481 Exposure Using Personal Passive Samplers. *Ann. Occup. Hyg.* 51, 121–130.
482 <https://doi.org/10.1093/annhyg/mel078>

483 Burns, A.M., Barlow, C.A., Banducci, A.M., Unice, K.M., Sahmel, J., 2019. Potential Airborne Asbestos
484 Exposure and Risk Associated with the Historical Use of Cosmetic Talcum Powder Products.
485 *Risk Anal.* 39, 2272–2294. <https://doi.org/10.1111/risa.13312>

486 Case, B.W., Abraham, J.L., Meeker, G., Pooley, F.D., Pinkerton, K.E., 2011. Applying Definitions of
487 “Asbestos” to Environmental and “Low-Dose” Exposure Levels and Health Effects, Particularly
488 Malignant Mesothelioma. *J. Toxicol. Environ. Health B Crit. Rev.* 14, 3–39.
489 <https://doi.org/10.1080/10937404.2011.556045>

490 Cattaneo, A., Gualtieri, A.F., Artioli, G., 2003. Kinetic study of the dehydroxylation of chrysotile asbestos
491 with temperature by in situ XRPD. *Phys. Chem. Miner.* 30, 177–183.
492 <https://doi.org/10.1007/s00269-003-0298-2>

493 Chimed-Ochir, O., Rath, E.M., Kubo, T., Yumiya, Y., Lin, R.-T., Furuya, S., Brislane, K., Klebe, S., Nowak,
494 A.K., Kang, S.-K., Takahashi, K., 2022. Must countries shoulder the burden of mesothelioma to
495 ban asbestos? A global assessment. *BMJ Glob. Health* 7, e010553.
496 <https://doi.org/10.1136/bmjgh-2022-010553>

497 Comba, P., Gianfagna, A., Paoletti, L., 2003. Pleural mesothelioma cases in Biancavilla are related to a
498 new fluoro-edenite fibrous amphibole. *Arch. Environ. Health* 58, 229–232.
499 <https://doi.org/10.3200/AEOH.58.4.229-232>

500 Décret 96-1133, 1996. Décret n°96-1133 du 24 décembre 1996 relatif à l’interdiction de l’amiante, pris
501 en application du code du travail et du code de la consommation, 96-1133.

502 Di Giuseppe, D.D., Zoboli, A., Nodari, L., Pasquali, L., Sala, O., Ballirano, P., Malferrari, D., Raneri, S.,
503 Hanuskova, M., Gualtieri, A.F., 2021. Characterization and assessment of the potential
504 toxicity/pathogenicity of Russian commercial chrysotile. *Am. Mineral.* 106, 1606–1621.
505 <https://doi.org/10.2138/am-2021-7710>

506 Dlg 257/92, 1992. Italian Law n. 257/92 (Legge 27 marzo 1992, n. 257 - Norme relative alla
507 cessazione dell’impiego dell’amianto). In *Suppl. Ord. alla Gazzetta Ufficiale* 87 del 13 aprile
508 1992.

509 DM September 06, 1994. Italian Ministry of Health - *Gazzetta Ufficiale della Repubblica Italiana* -
510 Normative e metodologie tecniche di applicazione dell’art.6, comma 3, e dell’art.12, comma 2,
511 della legge 27 marzo 1992, n.257, relativa alla cessazione dell’impiego dell’amianto.

512 Douglas, T., Van den Borre, L., 2019. Asbestos neglect: Why asbestos exposure deserves greater policy
513 attention. *Health Policy* 123, 516–519. <https://doi.org/10.1016/j.healthpol.2019.02.001>

514 Drnek, T., Moraes, M., Neto, P., 2018. Overview of magnesite. *J. Refract. Innov. RHIM Bull.* 1, 14–22.

515 EC 2006/1907, 2006. Regulation (EC) N. 1907/2006 of the European Parliament and of the Council of
516 18 December 2006 concerning the Registration, Evaluation, Authorisation and Restriction of
517 Chemicals (REACH), establishing a European Chemicals Agency, amending Directive
518 1999/45/EC and repealing Council Regulation (EEC) N. 793/93 and Commission Regulation
519 (EC) N. 1488/94 as well as Council Directive 76/769/EEC and Commission Directives
520 91/155/EEC, 93/67/EEC, 93/105/EC and 2000/21/EC.

521 EC 2009/148, 2009. Directive 2009/148/EC of the European Parliament and of the Council of 30
522 November 2009 on the protection of workers from the risks related to exposure to asbestos at
523 work.

524 Emory, T.S., Maddox, J.C., Kradin, R.L., 2020. Malignant mesothelioma following repeated exposures to
525 cosmetic talc: A case series of 75 patients. *Am. J. Ind. Med.* 63, 484–489.
526 <https://doi.org/10.1002/ajim.23106>

527 Finley, B.L., Pierce, J.S., Phelka, A.D., Adams, R.E., Paustenbach, D.J., Thuett, K.A., Barlow, C.A., 2012.
528 Evaluation of tremolite asbestos exposures associated with the use of commercial products.
529 *Crit. Rev. Toxicol.* 42, 119–146. <https://doi.org/10.3109/10408444.2011.636028>

530 Fitzgerald, S., Harty, E., Joshi, T.K., Frank, A.L., 2019. Asbestos in commercial indian talc. *Am. J. Ind.*
531 *Med.* 62, 385–392. <https://doi.org/10.1002/ajim.22969>

532 Fornasini, L., Raneri, S., Bersani, D., Mantovani, L., Scognamiglio, V., Di Giuseppe, D., Gualtieri, A.F.,
533 2022. Identification of iron compounds in chrysotile from the Balangero mine (Turin, Italy) by
534 micro-Raman spectroscopy. *J. Raman Spectrosc.* 53, 1931–1941.
535 <https://doi.org/10.1002/jrs.6434>

536 Frank, A.L., Joshi, T.K., 2014. The global spread of asbestos. *Ann. Glob. Health* 80, 257–262.
537 <https://doi.org/10.1016/j.aogh.2014.09.016>

538 Gemmi, M., Mugnaioli, E., Gorelik, T.E., Kolb, U., Palatinus, L., Boullay, P., Hovmöller, S., Abrahams, J.P.,
539 2019. 3D Electron Diffraction: The Nanocrystallography Revolution. *ACS Cent. Sci.* 5, 1315–
540 1329. <https://doi.org/10.1021/acscentsci.9b00394>

541 Gesetz 162, 1993. Gesetz zu dem Übereinkommen Nr. 162 der Internationalen Arbeitsorganisation
542 vom 24. Juni 1986 über Sicherheit bei der Verwendung von Asbest.

543 Gordon, R.E., Fitzgerald, S., Millette, J., 2014. Asbestos in commercial cosmetic talcum powder as a
544 cause of mesothelioma in women. *Int. J. Occup. Environ. Health* 20, 318–332.
545 <https://doi.org/10.1179/2049396714Y.0000000081>

546 Graf, D., 1961. Crystallographic tables for the rhombohedral carbonates. *American Mineralogist:*
547 *Journal of Earth and Planetary Materials.* *J. Earth Planet. Mater.* 46, 1283–1316.

548 Gualtieri, A.F., 2023. Journey to the centre of the lung. The perspective of a mineralogist on the
549 carcinogenic effects of mineral fibres in the lungs. *J. Hazard. Mater.* 442, 130077.
550 <https://doi.org/10.1016/j.jhazmat.2022.130077>

551 Gualtieri, A.F., 2020. Naturally Occurring Asbestos: A Global Health Concern? State of the Art and Open
552 Issues. *Environ. Eng. Geosci.* 26, 3–8. <https://doi.org/10.2113/EEG-2271>

553 Gualtieri, A.F. (Ed.), 2017. Mineral fibres: Crystal chemistry, chemical-physical properties, biological
554 interaction and toxicity, 1st ed. Mineralogical Society of Great Britain & Ireland.
555 <https://doi.org/10.1180/EMU-notes.18>

556 Gualtieri, A.F., 2000. Accuracy of XRPD QPA using the combined Rietveld–RIR method. *J. Appl.*
557 *Crystallogr.* 33, 267–278. <https://doi.org/10.1107/S002188989901643X>

558 Gualtieri, A.F., Gandolfi, N.B., Pollastri, S., Rinaldi, R., Sala, O., Martinelli, G., Bacci, T., Paoli, F., Viani, A.,
559 Vigliaturo, R., 2018. Assessment of the potential hazard represented by natural raw materials
560 containing mineral fibres—The case of the feldspar from Orani, Sardinia (Italy). *J. Hazard.*
561 *Mater.* 350, 76–87. <https://doi.org/10.1016/j.jhazmat.2018.02.012>

562 Gualtieri, A.F., Gatta, G.D., Arletti, R., Artioli, G., Ballirano, P., Cruciani, G., Guagliardi, A., Malferrari, D.,
563 Masciocchi, N., Scardi, P., 2019. Quantitative phase analysis using the Rietveld method:
564 Towards a procedure for checking the reliability and quality of the results. *Period. Mineral.* 88,
565 147–151. <https://doi.org/10.2451/2019PM870>

566 IARC, 2012. Asbestos (chrysotile, amosite, crocidolite, tremolite, actinolite, and anthophyllite, in: IARC
567 *Monogr. Eval. Carcinog. Risks. Hum.* IARC - International Agency for Research on Cancer, pp.
568 219–309.

569 Joshi, T.K., Bhuvra, U.B., Katoch, P., 2006. Asbestos Ban in India: Challenges Ahead. *Ann. N. Y. Acad. Sci.*
570 1076, 292–308. <https://doi.org/10.1196/annals.1371.072>

571 Khorami, J., Choquette, D., Kimmerle, F.M., Gallagher, P.K., 1984. Interpretation of EGA and DTG
572 analyses of chrysotile asbestos. *Thermochim. Acta* 76, 87–96. [https://doi.org/10.1016/0040-6031\(84\)87006-9](https://doi.org/10.1016/0040-6031(84)87006-9)

573

574 Kolb, U., Mugnaioli, E., Gorelik, T.E., 2011. Automated electron diffraction tomography - a new tool for
575 nano crystal structure analysis. *Cryst. Res. Technol.* 46, 542–554.
576 <https://doi.org/10.1002/crat.201100036>

577 Larson, A.C., Von Dreele, R.B., 1994. General Structure Analysis System (GSAS). Los Alamos National
578 Laboratory, Report LAUR 86-748.

579 Larson, T.C., Meyer, C.A., Kapil, V., Gurney, J.W., Tarver, R.D., Black, C.B., Lockey, J.E., 2010. Workers
580 with Libby amphibole exposure: retrospective identification and progression of radiographic
581 changes. *Radiology* 255, 924–933. <https://doi.org/10.1148/radiol.10091447>

582 Lemen, R., Landrigan, P., 2017. Toward an Asbestos Ban in the United States. *Int. J. Environ. Res. Public.*
583 *Health* 14, 1302. <https://doi.org/10.3390/ijerph14111302>

584 Lin, R.-T., Chien, L.-C., Jimba, M., Furuya, S., Takahashi, K., 2019. Implementation of national policies for
585 a total asbestos ban: a global comparison. *Lancet Planet. Health* 3, e341–e348.
586 [https://doi.org/10.1016/S2542-5196\(19\)30109-3](https://doi.org/10.1016/S2542-5196(19)30109-3)

587 Lister, J., Bailey, S., 1967. Chlorite polytypism: IV. Regular two-layer structures. *Am. Mineral.* 52, 1614–
588 1631.

589 Malferrari, D., Di Giuseppe, D., Scognamiglio, V., Gualtieri, A., 2021. Commercial brucite, a worldwide
590 used raw material deemed safe, can be contaminated by asbestos. *Period. Mineral.* Vol. 90 No. 3
591 (2021). <https://doi.org/10.13133/2239-1002/17384>

592 Manceau, A., Chateigner, D., Gates, W.P., 1998. Polarized EXAFS, distance-valence least-squares
593 modeling (DVLS), and quantitative texture analysis approaches to the structural refinement of
594 Garfield nontronite. *Phys. Chem. Miner.* 25, 347–365.
595 <https://doi.org/10.1007/s002690050125>

596 Marsili, D., Angelini, A., Bruno, C., Corfiati, M., Marinaccio, A., Silvestri, S., Zona, A., Comba, P., 2017.
597 Asbestos Ban in Italy: A Major Milestone, Not the Final Cut. *Int. J. Environ. Res. Public Health*
598 14, 1379. <https://doi.org/10.3390/ijerph14111379>

599 Mellini, M., 1982. The crystal structure of lizardite 1 T: hydrogen bonds and polytypism. *Am. Mineral.*
600 67, 587–598.

601 Ondrus, P., Veselovsky, F., Gabasova, A., Hlousek, J., Srein, V., Vavrin, I., Skala, R., Sejkora, J., Drabek, M.,
602 2003. Primary minerals of the Jachymov ore district. *J. Geosci.* 48, 19–147.

603 Petriglieri, J.R., Salvioli-Mariani, E., Mantovani, L., Tribaudino, M., Lottici, P.P., Laporte-Magoni, C.,
604 Bersani, D., 2015. Micro-Raman mapping of the polymorphs of serpentine: Micro-Raman
605 mapping of the polymorphs of serpentine. *J. Raman Spectrosc.* 46, 953–958.
606 <https://doi.org/10.1002/jrs.4695>

607 Pohl, W., 1990. Genesis of magnesite deposits — models and trends. *Geol. Rundsch.* 79, 291–299.
608 <https://doi.org/10.1007/BF01830626>

609 Rietveld, H., 1969. A profile refinement method for nuclear and magnetic structures. *J. Appl.*
610 *Crystallogr.* 2, 65–71.

611 Schlossman, M., 2009. *Chemistry and Manufacture of Cosmetics Volume 2: Formulating*, 4th ed.
612 Schlossman M.L., Allured Publishing Corporation.

613 Stanton, M.F., Layard, M., Tegeris, A., Miller, E., May, M., Morgan, E., Smith, A., 1981. Relation of particle
614 dimension to carcinogenicity in amphibole asbestoses and other fibrous minerals. *J. Natl.*
615 *Cancer Inst.* 67, 965–975.

616 Stanton, M.F., Wrench, C., 1972. Mechanisms of mesothelioma induction with asbestos and fibrous
617 glass. *J. Natl. Cancer Inst.* 48, 797–821.

618 Steinfink, H., Sans, F., 1959. Refinement of the crystal structure of dolomite. *Am. Mineral.* 44, 679–681.

619 Terracini, B., 2019. Contextualising the policy decision to ban asbestos. *Lancet Planet. Health* 3, e331–
620 e332. [https://doi.org/10.1016/S2542-5196\(19\)30134-2](https://doi.org/10.1016/S2542-5196(19)30134-2)

621 Thives, L.P., Ghisi, E., Thives Júnior, J.J., Vieira, A.S., 2022. Is asbestos still a problem in the world? A
622 current review. *J. Environ. Manage.* 319, 115716.
623 <https://doi.org/10.1016/j.jenvman.2022.115716>

624 Toby, B.H., 2001. EXPGUI, a graphical user interface for GSAS. *J. Appl. Crystallogr.* 34, 210–213.
625 <https://doi.org/10.1107/S0021889801002242>

626 Tzamos, E., Bussolesi, M., Grieco, G., Marescotti, P., Crispini, L., Kasinos, A., Storni, N., Simeonidis, K.,
627 Zouboulis, A., 2020. Mineralogy and Geochemistry of Ultramafic Rocks from Rachoni Magnesite
628 Mine, Gerakini (Chalkidiki, Northern Greece). *Minerals* 10, 934.
629 <https://doi.org/10.3390/min10110934>

630 Van Gossen, B., Lowers, H., Sutley, S., Gent, C., Castor, S., Papke, K., Meeuwig, R., 2003. Asbestos-bearing
631 talc deposits, southern Death Valley region, California, in: *Proceedings of the 39th Forum on*
632 *the Geology of Industrial Minerals*. Presented at the Betting on industrial minerals,
633 Reno/Sparks, Nevada, pp. 215–223.

634 Worliczek, E., 2017. Naturally Occurring Asbestos: The Perception of Rocks in the Mountains of New
635 Caledonia, in: Dürr, E., Pascht, A. (Eds.), *Environmental Transformations and Cultural*
636 *Responses*. Palgrave Macmillan US, New York, pp. 187–214. [https://doi.org/10.1057/978-1-](https://doi.org/10.1057/978-1-137-53349-4_8)
637 [137-53349-4_8](https://doi.org/10.1057/978-1-137-53349-4_8)

638 Yoon, Y.-R., Kwak, K., Choi, Y., Youn, K., Bahk, J., Kang, D.-M., Paek, D., 2018. The Asbestos Ban in Korea
639 from a Grassroots Perspective: Why Did It Occur? *Int. J. Environ. Res. Public. Health* 15, 198.
640 <https://doi.org/10.3390/ijerph15020198>

641

642

643 **Figure captions**

644

645 **Fig 1.** Graphical output of the Rietveld refinement of KT1 (a) and KG1 (b) powder samples.

646 Red crosses represent the observed pattern, the thin green line represents the calculated
647 pattern, and the blue bottom line is the difference line. The vertical bars mark of the peaks of
648 each crystalline phase included in the refinement procedure which are (from the bottom):
649 magnesite, dolomite, serpentine and quartz (a); magnesite, dolomite, serpentine, quartz, talc,
650 chlorite, calcite and smectite (b).

651

652 **Fig. 2.** Thermal behaviour of samples KT1. (a) TGA (solid lines) and DTG (dashed lines)
653 curves; (b) DTA curve (the maxima denote exothermic reactions); (c) MSEGAs for H₂O
654 (m/z=18) and CO₂ (m/z=44); the curves for NO (m/z=30) and SO₂ (m/z=64) are not reported
655 as these gasses were not detected.

656

657 **Fig. 3.** Macroscopic (a) and microscopic (b) observation of KT2 sample. (a) KT2 sample occurs
658 as centimetric fragments of grey-white rock with green veins (I); a magnification of the area
659 marked by the white arrow in (I) shows that the green veins are characterised by an
660 intergrowth of green plate-like mineral grains with white mineral fibre bundles highlighted by
661 the white arrows (II). (b) Chrysotile fibres observed with PCOM in bright (I) and (II) and dark
662 (III) and (IV) field. Fibres perpendicular to the polarizer, in bright field, have pale blue colour
663 and orange halo (I); fibres parallel to the polarizer, in bright field, have dark blue colour and
664 orange halo (II); fibres perpendicular to the polarizer, in dark field, have blue colour (III);
665 fibres parallel to the polarizer, in dark field, have purple colour (IV). The images (III) and (IV)

666 show the Walton-Beckett graticule (100 μm in diameter) to identify the length and width of
667 the fibres.

668 **Fig. 4.** Representative SEM images of Turkish and Greek magnesite samples: (a) flexible
669 chrysotile bundle with frayed and split ends dipped in a matrix of massive magnesite particles
670 in sample KT1; (b) detail of chrysotile fibres in magnesite fragments presents in sample KG1;
671 (c) elongated fibrous bundle with split ends in sample KT2; (d) detail of chrysotile fibres
672 dipped in a matrix massive magnesite particle in sample KG2; (e-f) representative EDX
673 spectra of the chrysotile fibres and magnesite particles shown in (a) and (b), respectively.

674

675 **Fig. 5.** Representative TEM images of the magnesite samples KT2 (a-e) and KG2 (f). (a) High-
676 angle annular dark-field images of chrysotile fibres; (b) A chrysotile fibre with a particularly
677 large channel of about 40 nm in diameter; (c) Massive fragments with composition, consistent
678 with serpentine minerals; (d) Reconstructed 3DED volume showing typical crowns of diffuse
679 scattering produced by the bending of the serpentine layers to form chrysotile; (e)
680 Reconstructed 3DED data set from a massive polygonal serpentine; (f) Examples of bent hair-
681 like fibres typically arranged in bundles.

682

683 **Fig. 6.** Raman spectra of KT1, KG1 and KT2 in the low-wavenumber (a) and in the OH-
684 stretching (b) spectral regions.

Table 1.

Qualitative phase analysis of the samples KT1, KG1, KT2, KG2, and VA.

Sample	Mineral phases
KT1	magnesite, dolomite, serpentine, quartz
KG1	magnesite, dolomite, smectite, quartz, serpentine, calcite, chlorite, talc
KT2	magnesite, dolomite, serpentine, quartz
KG2	magnesite, dolomite, serpentine
VA	magnesite

Table 2.

Mineralogical composition of KT1 and KG1 powder samples (wt%) obtained from the Rietveld quantitative phase analysis. The standard deviation σ_Q (values in parenthesis) of the weight percentage Q of each phase was also calculated in the GSAS software (Larson and Von Dreele, 1994).

Sample	KT1	KG1
R _{wp} (%)	13.4	14.8
R _p (%)	10	11.0
χ^2	7.5	9.3
magnesite	92.81(3)	92.43(3)
dolomite	4.7(1)	2.2(1)
quartz	0.67(4)	1.4(1)
talc	-	0.1(1)
chlorite	-	0.3(2)
calcite	-	0.5(1)
smectite	-	2.2(2)
serpentine	1.8(1)	0.8(2)

